Molecular Crystals and Liquid Crystals Incorporating Nonlinear Optics
Publication details, including instructions for authors and subscription information:
http://www.tandfonline.com/loi/gmcl17

Small Angle Neutron Scattering Studies of Polymer Orientation & Phase Separation

R. S. Stein [a]
[a] University of Massachusetts, Amherst, MA, 01003
Version of record first published: 22 Sep 2006.

To cite this article: R. S. Stein (1990): Small Angle Neutron Scattering Studies of Polymer Orientation & Phase Separation, Molecular Crystals and Liquid Crystals Incorporating Nonlinear Optics, 180:1, 119-146

To link to this article: http://dx.doi.org/10.1080/00268949008025794

Mol. Cryst. Liq. Cryst., 1990, Vol. 180A, pp. 119–146
Reprints available directly from the publisher
Photocopying permitted by license only

Printed in the United States of America

Small Angle Neutron Scattering Studies of Polymer Orientation & Phase Separation

R. S. STEIN

University of Massachusetts, Amherst, MA 01003

Small-Angle Neutron Scattering (SANS) studies are illustrated in three recent studies relevant to polymer properties. These are:

1. The study of the melt miscibility of linear and branched polyethylene.
2. The study of the morphologies arising from the crystallization of one or both components of a polymer mixture.
3. The measurement of the degree of chain extension in a highly oriented polymer.

In all of these studies, SANS contrast is enhanced using the isotope substitution technique in which an hydrogenous polymer is replaced in part by a corresponding deuterous polymer. Dimensions of molecules or lamellae are obtained from studies of the q variation of the scattered intensity (where $q = (4\pi/\gamma) \sin(\sigma/2)$), and compositions and interactions between components are deduced from quantitative measurements of absolute scattering intensities. The use of parallel-x-ray and light-scattering studies is illustrated.

POLYETHYLENE BLENDS

The miscibility of polymer blends has been explored using small angle neutron scattering (SANS). The occurrence of phase separation is conventionally studied by observation of a cloud point using visible light. It has been shown that a neutron scattering "cloud point" may also be used for this purpose.[1] This has the advantage that sufficient contrast can be obtained if one component is deuterium substituted so that it is sensitive in cases like those of polyethylene blends or blends of isomers of the same polymer (isostatic and atactic) where the small refractive index difference leads to low sensitivity of the optical measurement.

Through use of the de Gennes equation fused on the random phase approximation, the value of the Flory parameter, X, may be determined.

(1)

Here, ϕ_i, Z_i and $P_i(q)$ are the volume fraction, degree of polymerization, and single chain scattering function for component i and $R(q)$ is the Rayleigh ratio for scattering (identical with $d\Sigma/d\Omega$)[3]. From $P(q)$ the radius of gyration of a component may be obtained from

$$P(q)^{-1} = 1 + [\langle Rg^2 \rangle/3]q^2 + \ldots \quad (2)$$

By this means we have demonstrated miscibility of the melts of blends of linear polyethylene (HDPE) and branched polyethylene (LDPE) as well as HDPE and linear low density polyethylene (LLDE).[2] The values of X_{12} for these blends is small and positive but slightly below the critical X associated with molecular weights of the components used. It is likely that with higher molecular weights, temperature and degree of branching, immiscibility may be found in the melt.

In separate studies,[4,5,6] it is found that while the melts are miscible, those blends yield separate crystals which form mixed superstructures at the lamellar and spherulite levels.

POLY(VINYLADINE FLUORIDE)-POLY(METHYL-METHACRYLATE) BLENDS

In previous studies,[7,8,9] it has been shown that when a miscible blend of poly(vinylidene fluoride) (PVF_2) and Poly(methylmelharvylate) (PMMA) is crystallized, a morphology result is consisting of lamellar crystals of PVF_2 interspersed with a miscible amorphous blend of PVF_2 and PMMA. Evidence for this comes from small-angle X-ray scattering (SAXS) where it is found that

1. The repeat period increases with increasing PMMA content in a manner related to the increase in PMMA content of the PVF2 and PMMA.
2. The intensity of the SAXS increases with PMMA content in a manner that may be quantitatively related to the electron density, *re* of the amorphous layer. The SAXS invarient defined as

$$Q = \int R(q)q^2 df \tag{3}$$

can be described by

$$Q = k_2\phi_{cr}(1 - \phi_{cr})\,[\rho^e_{cr} - \rho^e_{am}]^2 \tag{4}$$

where ρ^e_{cr} is the electron density of the crystalline PVF_2 and

$$\rho^e_{am} = \phi_{PVF_2,am}\,\rho^e_{PVF_2,am} + \phi_{PMMA,am}\rho^e_{PMMA} \tag{5}$$

where ϕ_{PVF_2} and $\phi_{PMMA,QM}$ are the value fractions of PVF_2 and PMMA in the amorphous phase.

Recently, the groups of Wendorf and Yoon have postulated the existence of a transition layer of amorphous PVF_2 between the crystal and the amorphous blend. We find it difficult to determine whether this occurs using SAXS alone but have found it possible[10] to do so using deuterium substituted PMMA (*d*-PMMA) and with the SAXS invariants Q_x. In this case, assuming a three-phase model involving a crystalline (cv.) amorphous (am) and a transition'(tr) phase, the invariants are given by

$$Q_x = \phi_{cr}\,\phi_{am}\,(\rho^e_{cr} - \rho^e_{am})^2 + \phi_{cr}\,\phi_{tr}\,(\rho^e_{cr} - \rho^e_{tr})^2 + \phi_{am}\,\phi_{tr}\,(\rho^e_{am} - \rho^e_{tr})^2 \tag{6}$$

and

$$Q_N = \phi_{cr}\,\phi_{am}\,(A_{cr} - A_{am})^2 + \phi_{cr}\,\phi_{tr}\,(A_{cr} - A_{am})^2 + \phi_{am}\,\phi_{tr}\,(A_{am} - A_{tr})^2 \quad (7)$$

where the Q_i's and ρ_i^e's are the volume fractions and electron densities of the three phase, and A_i are the neutron scattering densities. We assume that ρ_{cr}^e and A_{cr} are values for the crystalline PVF_2, ρ_{tr}^e and A_{tr} are values for amorphous PVF_2 and ρ_{am}^e and A_{am} are values given for the blend where ρ_{am}^e is given by Equation (5) and A_{am} is given by the analogous equation.

$$A_{am} = \phi_{PFV_2,am}\,A_{PVF_2} + \phi_{PMMA}\,A_{PMMA} \quad (8)$$

where the a_i's are values for the amorphous phases and $\phi_{i,am}$ has been corrected for the presence of PVF_2 in the transition layer. It is noted that while a_{PMMA} is very dependent upon whether *d*-PMMA or *h*-PMMA is employed, ρ_{am}^e is not.

Thus Q_N should depend upon deuteration of PMMA but Q_x should not. Measurements using *d*-PMMA (obtained through the courtesy of E. L. duPont de Nemous, Inc.) demonstrate that while the form of the SAXS variation with of is independent of deuteration of the PMMA, the absolute SANS intensity (but not the SAXS intensity does not). Thus, it is possible to fit the invariants to Equations (6) and (7) and solve for ϕ_{cr}, ϕ_{am} and ϕ_{tr}.

Upon doing so, it is shown to be necessary to postulate the existence of the transition layer where ϕ_{tr} is of the order of 0.2 to 0.3. This is consistent with theoretical considerations of Yoon. It is not possible to distinguish between this three-phase model with amorphous phase separation and that of a gradient boundary where there is a concentration gradient in the amorphous phase ranging from pure, PVF_2 near the crystal to that of the blend.

Orientation studies

The measurement of anisotropy of radii of gyration has been demonstrated in other (Picot, Bove) and our laboratory.[11] By measuring $R(q)$ vs f in the plane and perpendicular to the plane of stretching, it is possible to determine $\langle R_y^2 \rangle$ parallel and perpendicular to the plane of (uniaxial) stretching.[11] Measurements on polystyrene (PS) (containing some deuterious PS) oriented using the capillary extrusion technique of R. S. Porter) demonstrates that for high molecular weight samples exhibit affine orientation, where the $\langle R \rangle_{rms}$ values change in the same ratio as do the dimensions of the sample. However, measurements on polyethylene[12,13,14] show less-than-affine molecular orientation. Also, whole $P(q)$ is Debye random coil function like for the unoriented sample, large deviations are seen, especially at large q. The observation of aggregation effects has been demonstrated by measurement of the molecular weight for the absolute $R(0)$ values for both oriented and unoriented samples. It is noted that a correction for slit desmearing is necessary for this for the oriented sample.[13,14]

It is not surprising that PE, being semi-crystalline is non-affine. The crystalline and amorphous regions undergo different orientation processes, and they are affected by degree of crystallization, morphology and chain topology.

We have applied this technique to ultra-oriented polyethylene samples crystallized using the gel technique. These were prepared using 2×10^6 molecular weight HDPE furnished through the courtesy of the Hinont Corp. and gel crystallized and oriented by P. Lemstra and measured at Oak Ridge National Laboratory.[15] The values of $\langle R_y^2 \rangle$ in the parallel direction are very large and not resolvable but values in the direction perpendicular to the direction of stretching are readily measurable. Values of $\langle R_y \rangle_{\text{rms}}$ less than 20–30 Å were obtained. These values, only with X-ray orientation data, suggest that molecules are almost completely oriented and that the disorientation of the various layers of films of samples used to obtain sufficient sample thickness for measurement was large compared with that occurring within a single film. Thus, the real value of $\langle R_m \rangle_{\text{rms}}$ (perpendicular) is probably less than the values specified above. It is proposed that it is better to look at a collection of films which are randomized in a plane perpendicular to the neutron beam. It is essential that this plane be oriented precisely in the perpendicular direction to avoid a contribution to the perpendicular radius of gyration from the very large length of the molecule. In this case, the length is so large as compared with the width, so that the observed q variation is primarily related to the width.

A preliminary measurement at LANSCE, at Los Alamos, is at least, qualitatively consistent with these results.[16]

We propose that the model of completely extended chains having imperfections of jogs and folds will serve to describe the perpendicular scattering data and will serve to characterize the defects.

These ultra-oriented samples, stretched in the range of 25x to 100x exhibit outstanding mechanical properties which vary with orientation procedures. Conventional methods for characterizing orientation involving X-ray diffraction, infrared dichroism and/or birefringence have little sensitivity in this regime of orientation. The mechanized behavior seems most related to this defect content which can be explored using SANS.

Acknowledgments

We appreciate the support of the National Science Foundation, the Office of Naval Research, and the Materials Research Laboratory of the University of Massachusetts in this work. We are also indebted to the Exxon Chemical Co. (Dr. F. Stehling), the E. D. duPont de Nenours, Inc. (Dr. Dkeda) and the Himont Corp. (Dr. T. Dziemanowicz) for providing samples, to Prof. R. S. Porter for extrusion orientation and Dr. P. Lemstra (University Eidhoven) for gel crystallization and orientation of polyethylene. We appreciate use of the facilities and collaborating with the Oak Ridge National Laboratory (Dr. G. Wignall), the National Bureau of Standards (Dr. C. Han), and the Los Alamos National Laboratory (Dr. P. Seeger) for SANS measurements.

PHASE SEPARATION IN BLENDS

- *Phase Separation in Amorphous Phase*
- *Crystallization*
- *Both Together*
- *Liquid Crystallization*

FIGURE 1 Phase separation in blends—its classification.

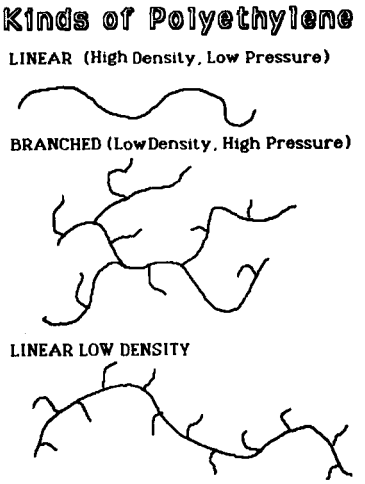

FIGURE 2 Types of polyethylene.

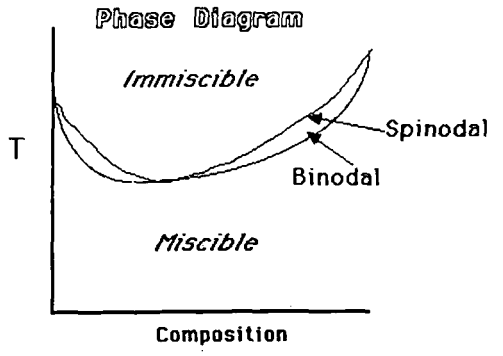

FIGURE 3 A typical binary amorphous blend phase diagram.

MELT MISCIBILITY OF PE BLENDS

o Neutron Cloud Points (Liquid-Liquid Phase Diagram)

$$I_{total}(T) \propto \int_{q_{min}}^{q_{max}} I(q, T)\, 2\pi q dq$$

or

$I(q_i, T)$ variation with T at a q_i

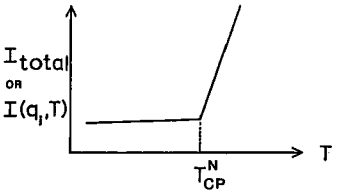

FIGURE 4 Neutron scattering cloud points.

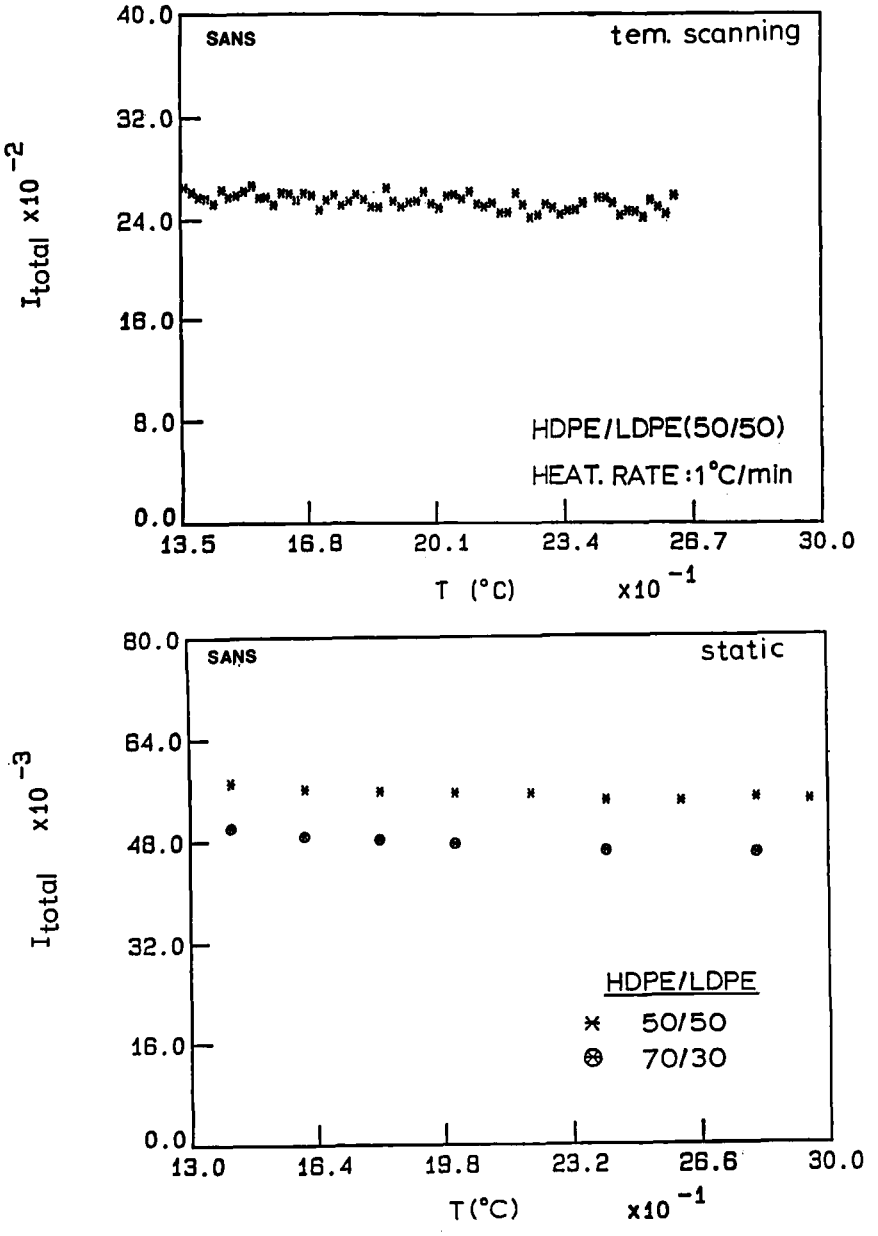

FIGURE 5 An attempt to find a neutron scattering cloud point for HDPE/LDPE blends.

o Interaction Parameter χ

$$\Delta G_{mix} = \Delta H_{mix} - T\Delta S_{mix}$$

$$\Delta G_{mix} = RT\left[\frac{\phi_1}{Z_1}\ln\phi_1 + \frac{\phi_2}{Z_2}\ln\phi_2 + \underbrace{\chi\phi_1\phi_2}_{\Gamma = g\phi_1\phi_2}\right]$$

$$\left.\begin{array}{l}\Delta G_{mix} < 0 \\ \dfrac{\partial^2 \Delta G_{mix}}{\partial \phi_2^2} > 0\end{array}\right\} \quad \text{miscible condition}$$

$$R_C^{-1}(o,T) \propto \partial^2 \Delta G_{mix}/\partial\phi_2^2$$

* Modified Zimm Equation (Stein et al.)
* de Gennes Scattering Function with RPA
* Extended Ornstein-Zernike Theory (Benoit et al.)

FIGURE 6 Thermodynamics of phase miscibility.

$$R_C \rightarrow \{\phi Z[P(q) + NQ(q)]\} = \left[\frac{1}{\phi Z P^{\circ}(q)} + \frac{1}{(1-\phi)Z_S P_S^{\circ}(q)} - 2\chi\right]^{-1}$$

- fit the above equation with Debye functions (for $P^{\circ}(q)$ and $P_S^{\circ}(q)$) and adjustable χ
- Zimm plot;

$$\{\phi Z[P(q) + NQ(q)]\}^{-1} = b_o + b_1 q^2 \ (+ b_2 q^4)$$

$$b_o = 1/\phi Z + 1/[(1-\phi)Z_S] - 2\chi$$

$$= 2(\chi_S - \chi)$$

- Limit of stability of miscible single phase;

$$\chi \leq \chi_S$$

FIGURE 7 The random phase approximation approach.

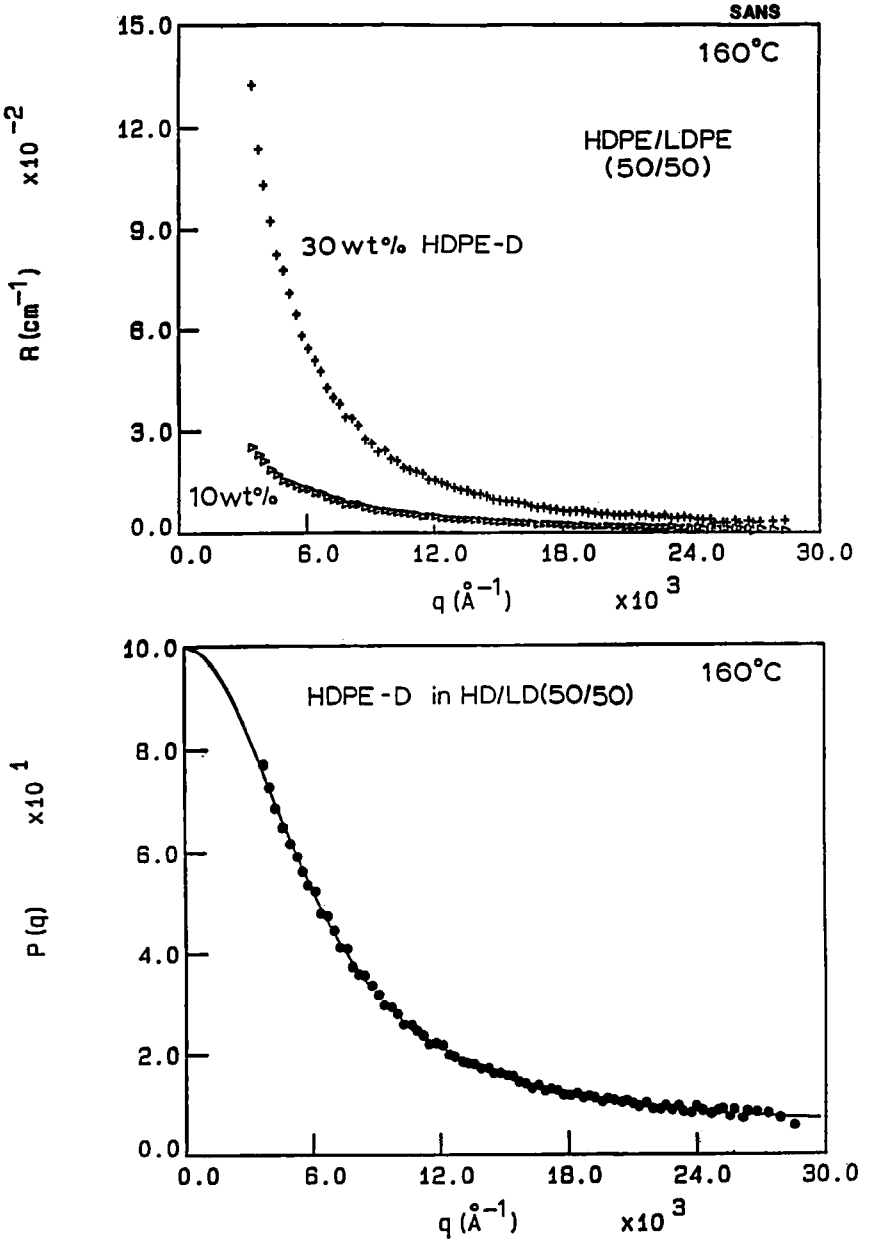

FIGURE 8 Typical SANS data for a HDPE/LDPE blend.

MOLECULAR DIMENSIONS OF THE HDPE-D COMPONENT IN THE BLENDS MEASURED BY SANS

	(w/w)	T (°C)	$(R_g^2)_z^{1/2}$ ±5%Å	$(R_g^2)_w^{1/2}$ ±5%Å	M_w^*
HDPE/LDPE	50/50	160	265	215	218, 500
HDPE/LDPE	50/50	180	266	216	220, 500
HDPE-D/HDPE	10/90	160	266	216	220, 500

* $Mw = Z_D m_H$

INTERACTION PARAMETERS OF THE POLYETHYLENE BLENDS OBTAINED BY SANS

	(W/W)	T (°C)	χ x 10^4	χ_S x 10^4	x/v_o x 10^6	x_s/v_o x 10^6	x/x_s
HDPE/LDPE (TERNARY)	50/50	160	2.16	2.36	6.56	7.18	0.914
HDPE/LDPE (TERNARY)	50/50	180	2.18	2.36	6.62	7.18	0.923
HDPE/LDPE (BINARY)	50/50	160	2.28	2.36	6.94	7.18	0.967

FIGURE 9 Molecular parameters obtained from SANS for a HDPE/LDPE blend.

CONCLUSION

- No neutron cloud point was observed over 150 °C - 300 °C.
- HDPE and LDPE are miscible at 150 °C - 300 °C range.
- If UCST and LCST exist in the HDPE/LDPE blend, UCST may be far below melting point while LCST may exist above 300 C or above degradation temperature.
- The components in the HDPE/LDPE blend crystallize separately at levels of crystallite and lamella.

FIGURE 10 Conclusions from polyethylene blend studies.

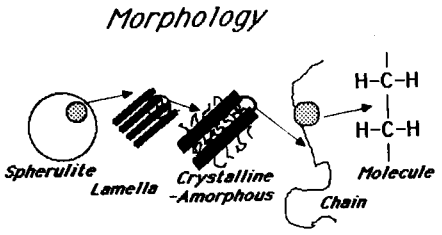

FIGURE 11 Hierarchy of morphologies for crystalline polymers.

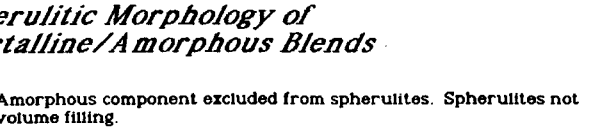

FIGURE 12 Spherulitic morphology of crystalline/amorphous blends.

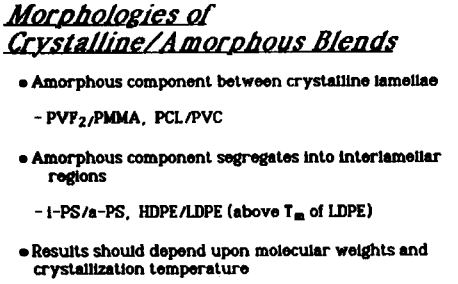

FIGURE 13 Morphology of crystalline/amorphous blends.

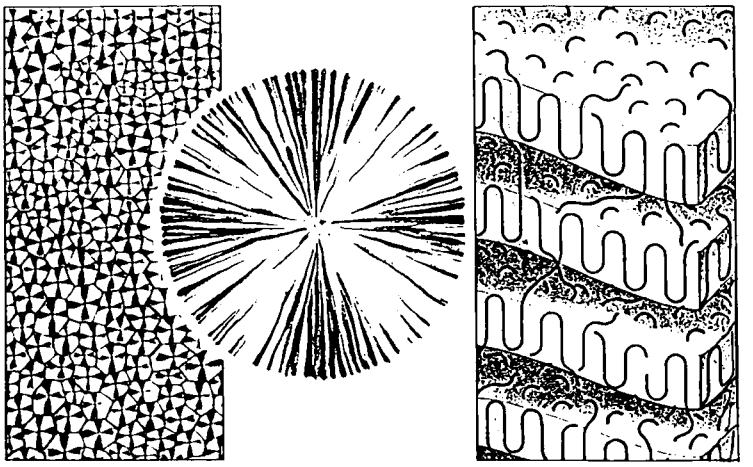

MICROSTRUCTURE OF A SEMICRYSTALLINE POLYMER such as polyethylene is shown at three levels of detail. Under polarized light such polymers are usually found to be made up of closely packed spherulites: sunburstlike structures formed as the polymer solidified and crystal growth began at nucleation points and radiated outward. Spherulites commonly grow to diameters of between tens and hundreds of micrometers (millionths of a meter). On a finer scale each spherulite is a radial assemblage of narrow crystalline plates oriented in many different planes. Within each of the lamellae, or plates, tightly packed polymer chains fold back and forth between two boundaries; amorphous regions where molecules are tangled and disarranged fill spaces between lamellae.

FIGURE 14 The morphology of spherulites (from E. Baer, Scientific American).

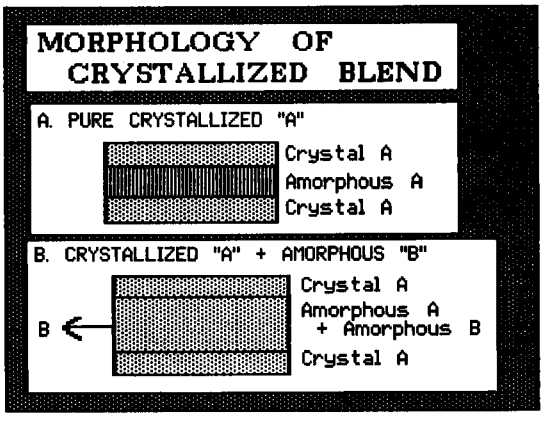

FIGURE 15 Lamellar morphology of crystalline/amorphous blends.

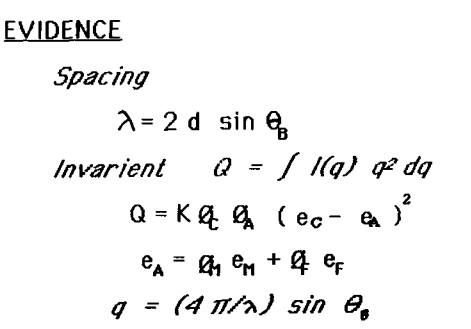

FIGURE 16 Evidence for lamellar morphology.

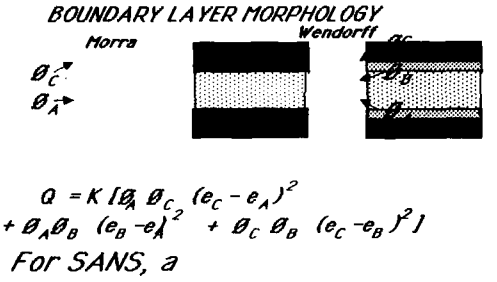

FIGURE 17 Two-phase vs. three phase model.

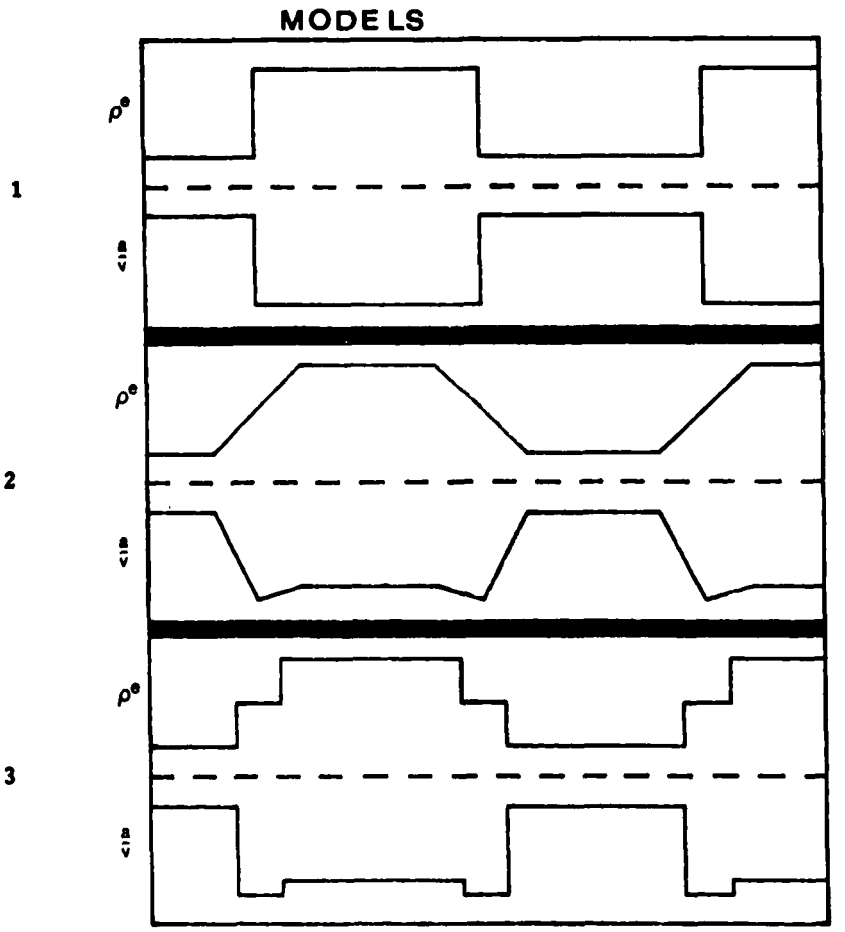

FIGURE 18 Electron density and neutron scattering lengths for three models of PVF_2/PMMA blends.

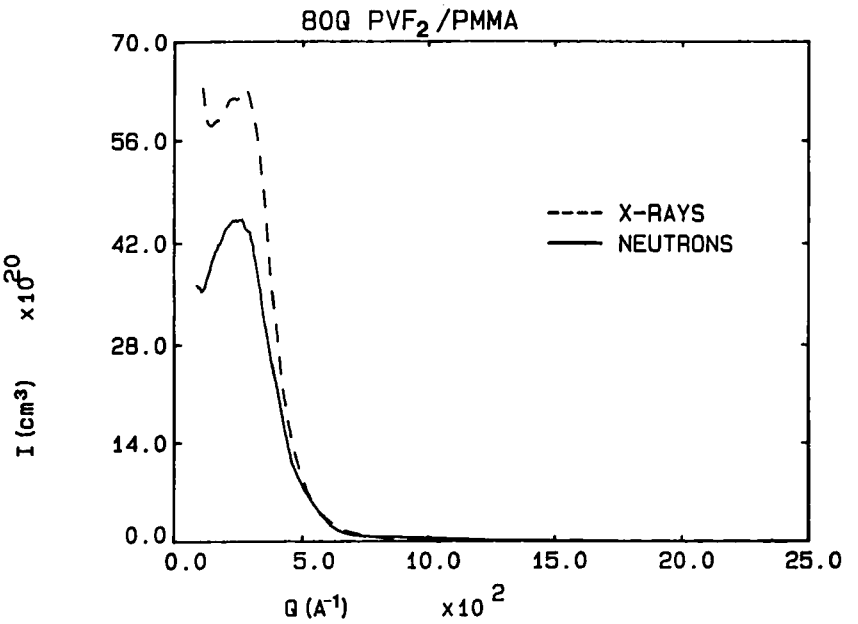

FIGURE 19 SANS and SAXS data for a PVF_2/PMMA blend.

MODEL 1

	ϕ_{max}(SAXS)	ϕ_{max}(SANS)
90Q	.71	.48
80Q	.55	.34
70Q	.45	.29
90M	.72	.52
80M	.55	.35
70M	.46	.29

FIGURE 20 A test of the two phase model.

MODEL 3.

	$\phi_{e\,(inv)}$	$\phi_{e(Porod)}$	ϕ_A	ϕ_C
90Q	.27±.08	.10	.30±.04	.43±.08
80Q	.24±.06	.13	.43±.04	.33±.06
70Q	.20±.04	.15	.56±.04	.24±.04
90M	.25±.08	.10	.32±.04	.43±.08
80M	.23±.06	.14	.44±.04	.33±.06
70M	.18±.04	.13	.56±.04	.26±.04

FIGURE 21 Data fitting parameters for the three-phase model.

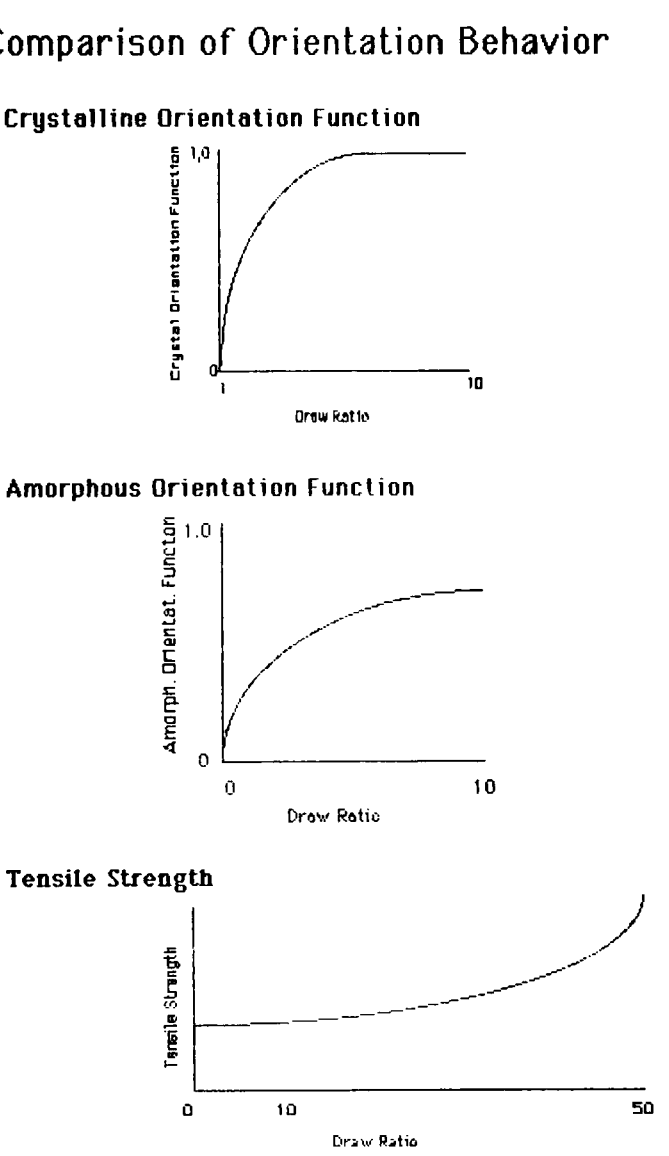

FIGURE 22 Variation of crystalline and amorphous orientation and tensile strength with orientation.

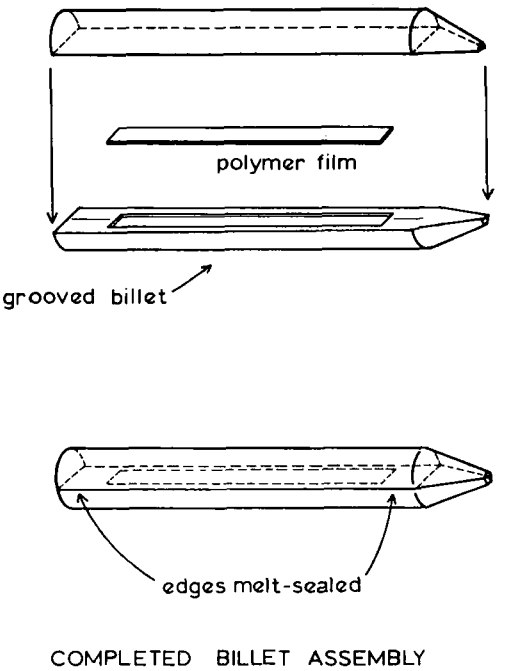

FIGURE 23 Split billet technique for polymer orientation (R. S. Porter).

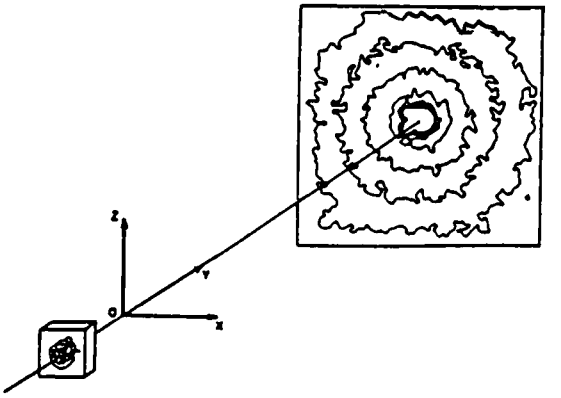

1. Geometry of SANS experiment and intensity contour plot for scattering from the unoriented amorphous polystyrene. The difference between the normalized intensity of the outer and the inner contour levels is about 200.

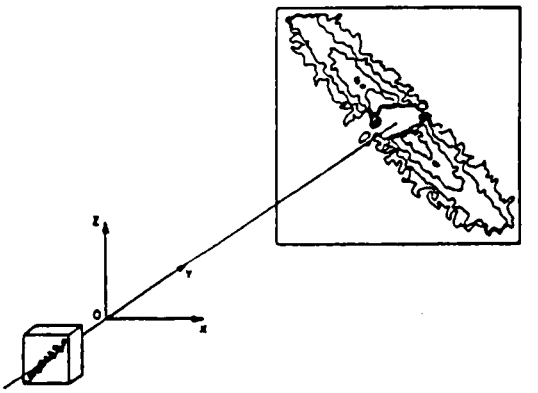

Geometry of SANS experiment and intensity contour plot for scattering from the oriented amorphous polystyrene, EDR = 4.2. The difference between the normalized intensity of the outer and the inner contour levels is about 100.

FIGURE 24 SANS contour diagrams for unoriented and oriented deuterium labelled polystyrene.

RESULTS AND DISCUSSION

A Zimm plot of $I^{-1}(q)$ vs. q^2 allows the determination of the radius of gyration and the molecular weight

$$I^{-1}(q) = \frac{1}{C\,M}\left(1 - \frac{q^2 Rg^2}{3}\right)$$

Slices of the scattering pattern parallel and perpendicular to the draw direction were analyzed separatly to determine $Rg_{\parallel}$ and $Rg_{\perp}$

FIGURE 25 Determination of R_g by Zimm analysis for oriented polymers.

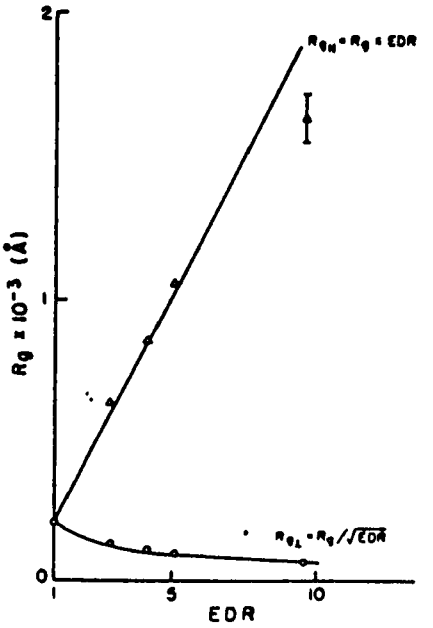

Radius of gyration as a function of EDR: (O) transversal radius of gyration, $(R_g)_{\perp}$; (Δ) longitudinal radius of gyration, $(R_g)_{\parallel}$. The continuous lines represent the variations of the radius of gyration assuming an affine transformation and constant volume.

FIGURE 26 Variation of R_g in the parallel and perpendicular directions for oriented polystyrene and polyethylene.

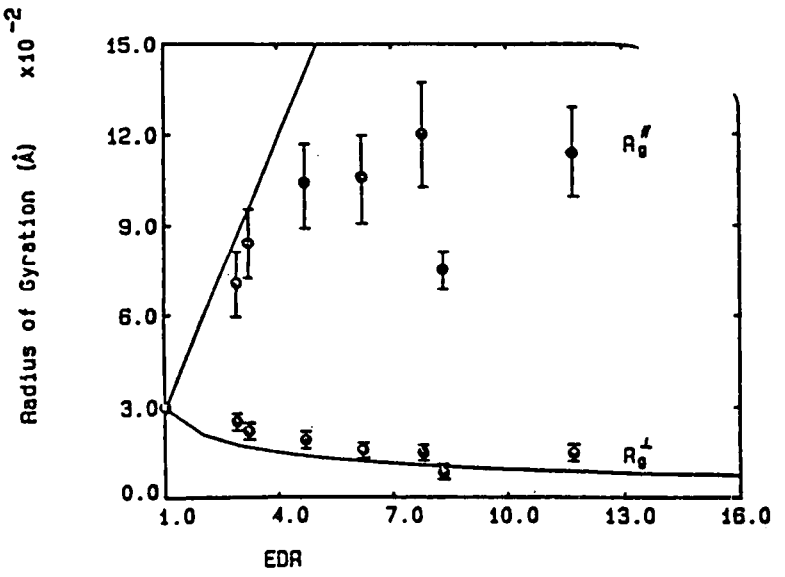

FIGURE 26 (*continued*)

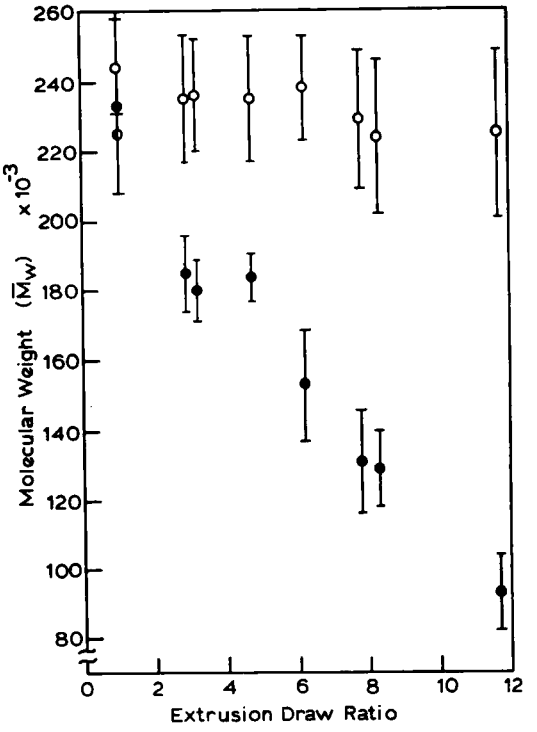

FIGURE 27 Variation of SANS determined molecular weight with elongation for polyethylene—effect of desmearing.

Table 2. Comparison of Tensile Moduli in Order of Increasing Approximate Ambient Values

Material	Modulus, $\times 10^{-10}$ dynes/cm^2	Polyethylene
Bulk polymers	1-7	Bulk polyethylene
Aluminum alloys	<70	↓
Glass filaments	70-85	Special strands
Other polymer limits	<125	
All steels	~200	↓
Polyethylene limit	240	Continuous crystals
Carbon filaments	240 → 500	

FIGURE 28 Elastic moduli for various materials.

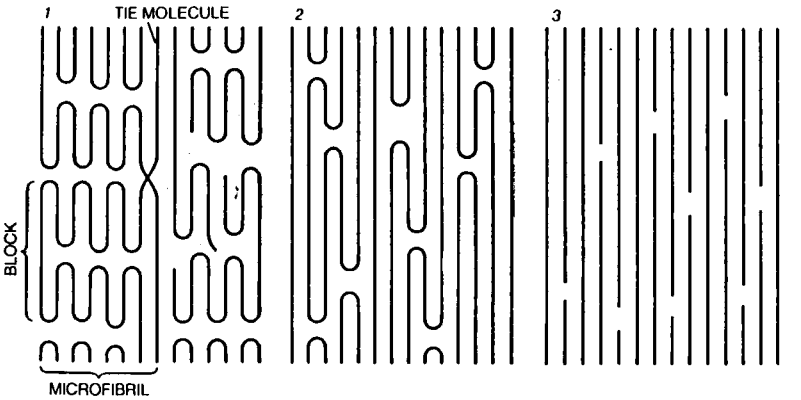

ALIGNMENT OF POLYMER CHAINS lends tensile strength to a fiber drawn from a semicrystalline polymer. During the initial stretching the crystalline lamellae in the polymer break up into smaller blocks of folded chains, which line up end to end to form numerous distinct microfibrils (*1*). The blocks are linked by extended tie molecules, which strengthen the microfibrils. More extensive stretching of the polymer partially unfolds the blocks and causes the microfibrils to merge (*2*). The greater number of molecules that are extended along the axis of the fiber further strengthen it. In an ideal morphology all the polymer chains would lie along the axis of the fiber (*3*), and the fiber would benefit fully from the great longitudinal strength of the polymer macromolecules.

FIGURE 29 Chain unfolding during stretching of a crystalline polymer (from E. Baer, Scientific American).

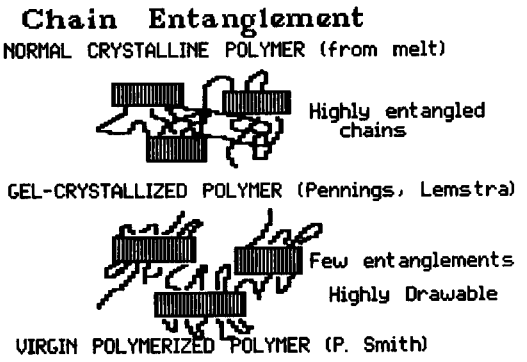

FIGURE 30 Entangled and disentangled structures for crystalline polymers.

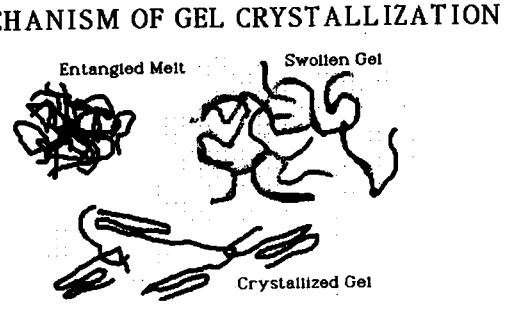

FIGURE 31 Mechanism of gel crystallization.

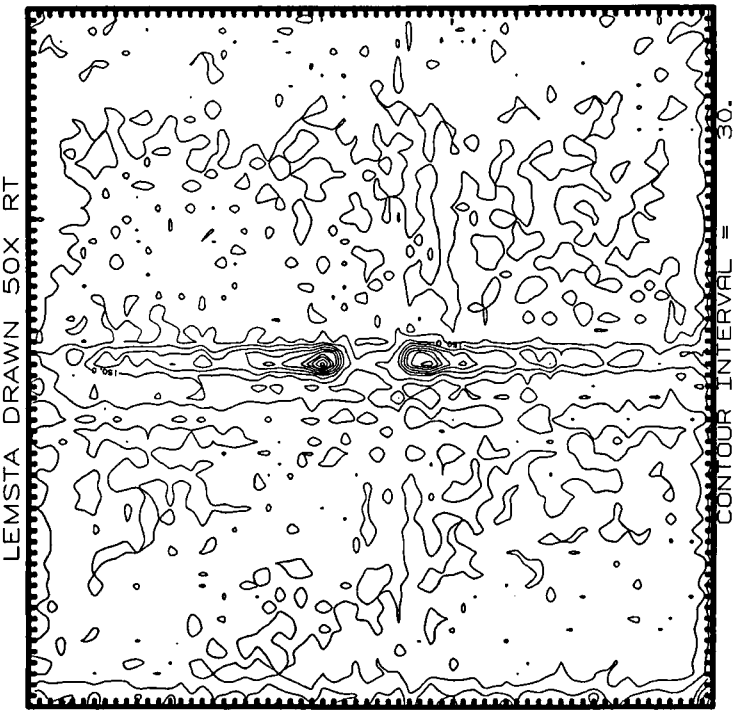

FIGURE 32 A typical SANS contour diagram (ORNL) for 50X drawn deuterium labelled gel crystallized polyethylene.

CONCLUSIONS

* For coextruded HDPE, the deformation is non-affine for draw ratios > 4

* Rg show a leveling off at draw ratios > 8 at 120 Å.

* For gel- crystalized UHMW PE, $Rg_{\perp}$ is much lower (40 Å), indicating far more molecular extention.

* Molecular modeling might be used to determine chain dimensions at large q regions by categorizing the various chain defects.

FIGURE 33 Conclusions from polyethylene orientation studies.

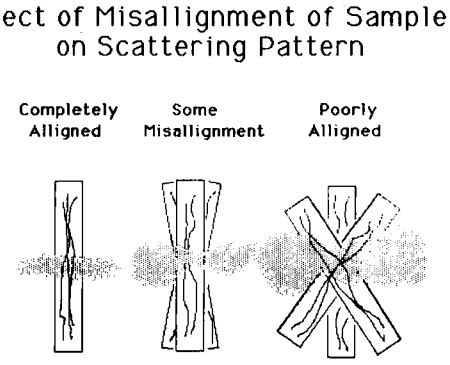

FIGURE 34 Smearing resulting from sample misorientation.

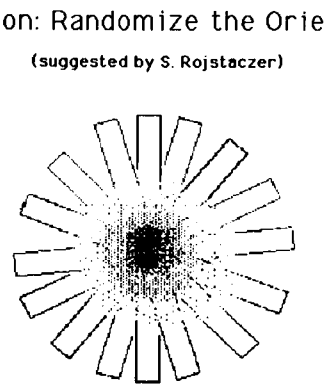

FIGURE 35 Circular averaging for an oriented sample.

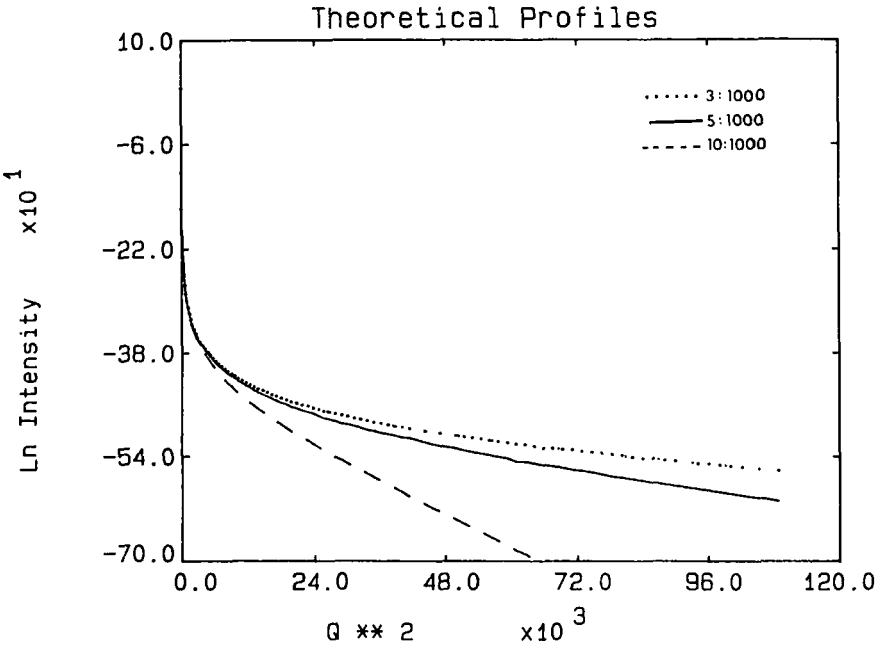

FIGURE 36 Calculate scattering curves for circularly averaged samples for various values of L/W.

Theoretically, it is possible to calculate the scattering pattern directly from the atomic coordinates.

$$I(q) = \sum_i \sum_j f_i f_j \cos(\vec{q} \cdot \vec{r}_{ij})$$

This has been done for simple defects, such as jogs and folds, and for short chain lengths. The structures were cylindrically averaged about the center of mass, and scattering perpendicular to the draw direction was calculated.

FIGURE 37 The molecular calculation of $S(q)$.

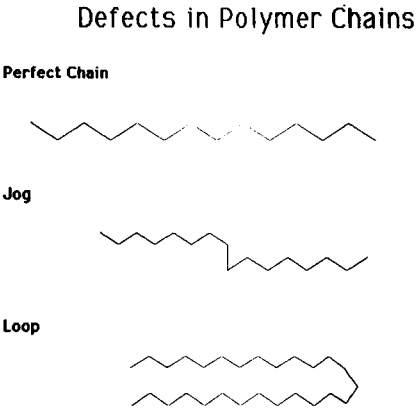

FIGURE 38 Postulated defects on almost completely oriented polyethylene.

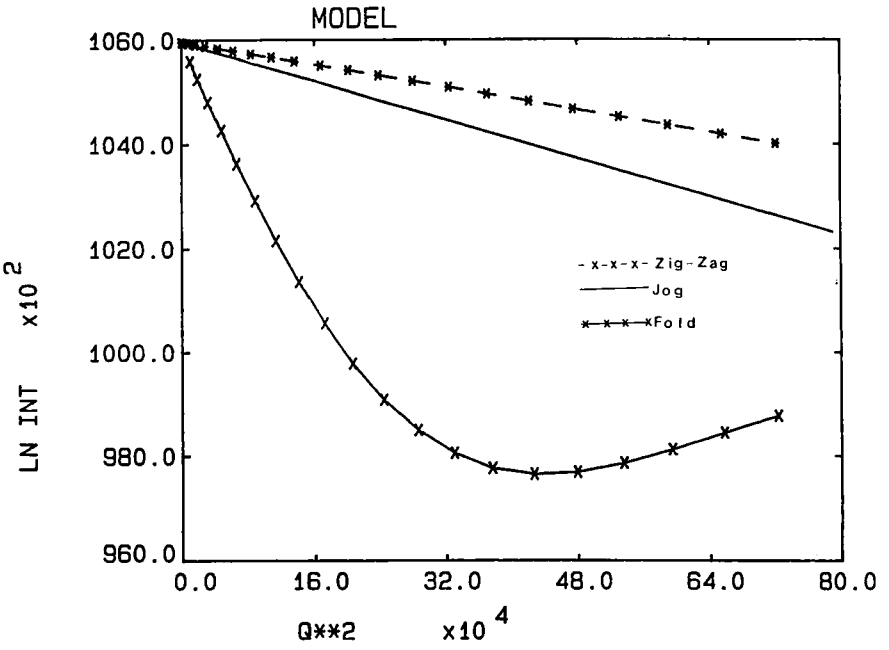

FIGURE 39 Calculated S(q) (perpendicular) curves for perfect polyethylene chains and those containing a randomly located jog or fold.

References

1. H. Yuny, M. Shibuyuma, C. C. Hun, and R. S. Stein, *Polymer Bull.*, **12**, 7 (1904).
2. M. Ree, PhD Thesis, Univ. of Mass., Amherst, MA, 1987, submitted to Macromolecules.
3. G. Hadziioannov and R. S. Stein, *Macromolecules*, **17**, 567 (1984).
4. S. R. Hu, T. Kyv and R. S. Stein, *J. Polym. Sci., Phys. Ed.*, **25**, 71 (1987).
5. T. Kyv, S. R. Hu, and R. S. Stein, *J. Polym. Sci., Polym. Phys. Ed.*, **25**, 89 (1987).
6. M. Ree, T. Kyv, and R. S. Stein, *J. Polym. Sci. Polym. Phys. Ed.*, **25**, 105 (1987).
7. B. S. Morra, PhD Thesis, Univ. of Mass., Amherst, MA (1981).
8. B. S. Morra, *J. Polym. Sci., Polym. Phys. Ed.*, **2243**, 2261 (1982).
9. B. S. Morra and R. S. Stein, *Polym. Eng. Sci.*, **24**, 311 (1984).
10. W. Herman, PhD Thesis, Univ. of Mass., Amherst, MA (1987).
11. G. Hadziioannov, L. H. Wang, R. S. Porter and R. S. Stein, *Macromolecules*, **11**, 880 (1982).
12. R. S. Stein, *Mat. Res. Soc. Proc.*, **79**, 3 (1987).
13. R. Lo, PhD Thesis, Univ. of Mass., Amherst, MA (1987).
14. R. Lo, A. Hill and R. S. Stein, *Macromolecules*, in press.
15. S. Roy, M. Satkowski and R. S. Stein, to be submitted for publication.
16. P. Seeger, personal communication.